Research Article | Vol. 8, No. 4 | 1 Apr 2018 | OPTICAL MATERIALS EXPRESS 919
Optical Materials EXPRESS

Compact refractive index sensor based on an S-tapered fiber probe

CHAO CHEN,[1,4] RUI YANG,[2] XUAN-YU ZHANG,[3] WEI-HUA WEI,[3] QI GUO,[3] XING ZHANG,[1] LI QIN,[1] YONG-QIANG NING,[1] AND YONG-SEN YU[3,5]

[1]*State Key Laboratory of Luminescence and Application, Changchun Institute of Optics, Fine Mechanics and Physics, Chinese Academy of Sciences, Changchun 130033, China*
[2]*Beijing Aerospace Yilian Science & Technology Development Co., Ltd, Beijing 100176, China*
[3]*State Key Laboratory on Integrated Optoelectronics, College of Electronic Science and Engineering, Jilin University, 2699 Qianjin Street, Changchun 130012, China*
[4]*chenc@ciomp.ac.cn*
[5]*yuys@jlu.edu.cn*

Abstract: We have demonstrated a refractive index (RI) sensor based on an S-tapered fiber probe (STFP) with a silver mirror on its end facet. The fiber probe has a compact size of about 1 mm, making it proper for sensing in narrow or limited space. The reflection spectra of the STFPs with different structure lengths have been analyzed and simulated. Its RI sensitivity in the range of 1.332 ~1.387 reaches 268.8 nm/RI unit, which is 9 times higher than that of the existing reflective fiber-taper-based RI sensor. Furthermore, the thermal response experimental results show that the STFP is temperature insensitive.

OCIS codes: (060.2370) Fiber optics sensors; (060.2280) Fiber design and fabrication; (060.2310) Fiber optics.

References and links

1. B. H. Lee, Y. H. Kim, K. S. Park, J. B. Eom, M. J. Kim, B. S. Rho, and H. Y. Choi, "Interferometric fiber optic sensors," Sensors (Basel) **12**(3), 2467–2486 (2012).
2. A. Cusano, D. Paladino, and A. Iadicicco, "Microstructured fiber Bragg gratings," J. Lightwave Technol. **27**(11), 1663–1697 (2009).
3. S. W. James and R. P. Tatam, "Optical fibre long-period grating sensors: characteristics and application," Meas. Sci. Technol. **14**(5), R49–R61 (2003).
4. P. Vaiano, B. Carotenuto, M. Pisco, A. Ricciardi, G. Quero, M. Consales, A. Crescitelli, E. Esposito, and A. Cusano, "Lab on fiber technology for biological sensing applications," Laser Photonics Rev. **10**(6), 922–961 (2016).
5. T. Guo, "Fiber grating-assisted surface plasmon resonance for biochemical and electrochemical sensing," J. Lightwave Technol. **35**(16), 3323–3333 (2017).
6. W. Liang, Y. Y. Huang, Y. Xu, R. K. Lee, and A. Yariv, "Highly sensitive fiber Bragg grating refractive index sensors," Appl. Phys. Lett. **86**(15), 151122 (2005).
7. C. Chen, Y. S. Yu, R. Yang, C. Wang, J. C. Guo, Y. Xue, Q. D. Chen, and H. B. Sun, "Reflective optical fiber sensors based on tilted fiber Bragg gratings fabricated with femtosecond laser," J. Lightwave Technol. **31**(3), 455–460 (2013).
8. T. Allsop, R. Arif, R. Neal, K. Kalli, V. Kundrát, A. Rozhin, P. Culverhouse, and D. J. Webb, "Photonic gas sensors exploiting directly the optical properties of hybrid carbon nanotube localized surface plasmon structures," Light Sci. Appl. **5**(2), e16036 (2016).
9. M. Śmietana, M. Koba, P. Mikulic, and W. J. Bock, "Towards refractive index sensitivity of long-period gratings at level of tens of μm per refractive index unit: fiber cladding etching and nano-coating deposition," Opt. Express **24**(11), 11897–11904 (2016).
10. O. Frazão, J. L. Santos, F. M. Araújo, and L. A. Ferreira, "Optical sensing with photonic crystal fibers," Laser Photonics Rev. **2**(6), 449–459 (2008).
11. D. K. Wu, B. T. Kuhlmey, and B. J. Eggleton, "Ultrasensitive photonic crystal fiber refractive index sensor," Opt. Lett. **34**(3), 322–324 (2009).
12. A. Schwuchow, M. Zobel, A. Csaki, K. Schröder, J. Kobelke, W. Fritzsche, and K. Schuster, "Monolayers of different metal nanoparticles in microstructured optical fibers with multiplex plasmonic properties," Opt. Mater. Express **2**(8), 1050–1055 (2012).
13. N. Zhang, G. Humbert, Z. Wu, K. Li, P. P. Shum, N. M. Y. Zhang, Y. Cui, J. L. Auguste, X. Q. Dinh, and L. Wei, "In-line optofluidic refractive index sensing in a side-channel photonic crystal fiber," Opt. Express **24**(24), 27674–27682 (2016).

#317918 https://doi.org/10.1364/OME.8.000919
Journal © 2018 Received 18 Dec 2017; revised 11 Feb 2018; accepted 12 Feb 2018; published 15 Mar 2018

Optical Materials EXPRESS

14. J. Zhang, Q. Sun, R. Liang, J. Wo, D. Liu, and P. Shum, "Microfiber Fabry-Perot interferometer fabricated by taper-drawing technique and its application as a radio frequency interrogated refractive index sensor," Opt. Lett. **37**(14), 2925–2927 (2012).
15. Q. Sun, H. Luo, H. Luo, M. Lai, D. Liu, and L. Zhang, "Multimode microfiber interferometer for dual-parameters sensing assisted by Fresnel reflection," Opt. Express **23**(10), 12777–12783 (2015).
16. Z. Tian, S. S. H. Yam, J. Barnes, W. Bock, P. Greig, J. M. Fraser, H. P. Loock, and R. D. Oleschuk, "Refractive index sensing with Mach-Zehnder interferometer based on concatenating two single-mode fiber tapers," IEEE Photonics Technol. Lett. **20**(8), 626–628 (2008).
17. Y. Miao, X. Ma, J. Wu, B. Song, H. Zhang, K. Zhang, B. Liu, and J. Yao, "Low-temperature cross-talk magnetic-field sensor based on tapered all-solid waveguide-array fiber and magnetic fluids," Opt. Lett. **40**(16), 3905–3908 (2015).
18. S. L. Fu, H. H. Dai, Q. G. Shi, and B. J. Peng, "A refractive index sensor based on the tapering theory," IEEE Sens. J. **16**(4), 954–957 (2016).
19. Z. Tian, S. S. H. Yam, and H. P. Loock, "Refractive index sensor based on an abrupt taper Michelson interferometer in a single-mode fiber," Opt. Lett. **33**(10), 1105–1107 (2008).
20. Y. Li, L. Chen, E. Harris, and X. Bao, "Double-pass in-line fiber taper Mach-Zehnder interferometer sensor," IEEE Photonics Technol. Lett. **22**(23), 1750–1752 (2010).
21. R. Yang, Y. S. Yu, Y. Xue, C. Chen, Q. D. Chen, and H. B. Sun, "Single S-tapered fiber Mach-Zehnder interferometers," Opt. Lett. **36**(23), 4482–4484 (2011).
22. R. Yang, Y. S. Yu, C. Chen, Y. Xue, X. L. Zhang, J. C. Guo, C. Wang, F. Zhu, B. L. Zhang, Q. D. Chen, and H. B. Sun, "S-tapered fiber sensors for highly sensitive measurement of refractive index and axial strain," J. Lightwave Technol. **30**(19), 3126–3132 (2012).
23. H. F. Taylor, "Bending effects in optical fibers," J. Lightwave Technol. **2**(5), 617–628 (1984).

1. Introduction

For decades, optical fiber sensors have attracted lots of interests in various physical, chemical and biological sensing applications due to their merits of small size, fast response, corrosion resistance, and biocompatibility [1–3]. Among them, fiber refractive index (RI) sensors have been intensively studied in recent years, because RI itself is an important physical parameter and many other biochemical parameters, such as solution concentration and pH value, can be measured based on RI change [4, 5]. To date, variety of fiber RI sensors have been developed, for example, fiber Bragg gratings (FBGs) [2, 6–8], long period fiber gratings (LPFGs) [3, 9], microstructured optical fibers (MOFs) [10–13], micro/nano fiber [14, 15], fiber-taper-based interferometers [16–22], and so on. The fiber-grating-based (FBGs and LPFGs) RI sensors have high resolution and a large detection range, but they require precise and expensive fabrication methods, including phase mask and laser source. The MOFs have high RI sensitivity, but the analytes need to be filled into the microholes of the fiber for each measurement, seriously complicating the test process. Micro/nanofiber sensor is also one of the best choices to realize highly sensitive RI measurement, which can achieve stronger evanescent field, but the mechanical strength and stability of the device will be reduced. The fiber-taper-based RI sensors in conventional optical fibers have advantages of simple structure, ease of fabrication and low cost, but their RI sensitivities are not satisfyingly high, and they usually have a large structure size with the total length of tens of millimeters, which is not compact for integrated applications. Recently, a novel RI sensor based on a single "S"-like fiber taper has been reported [21, 22]. The S fiber taper (SFT) sensor has a small size (less than 1 mm) and a high RI sensitivity. But its ultra-high axial strain sensitivity may affect the measurements when the structure has a small bending. In addition, like most of the fiber-taper-based Mach-Zehnder interferometers (MZIs) [16–18], the SFT works in the transmission mode, which is not flexible compared with the reflection-type sensors and limits its practical applications especially when the detection is required in some narrow or limited space, such as small-bore chemical containers or human blood vessels. However, the existing fiber-taper-based reflection-type RI sensors [19, 20] are too long to form a compact fiber probe.

In this paper, we propose a RI sensor based on the reflection-type S-tapered fiber probe (STFP), which has a silver mirror on the cleaved fiber end facet next to the SFT. The STFP has a short structure length of about 1 mm, which is more flexible in practical applications and is not easy to bend, avoiding the cross-sensitivity of structure bending. When the STFP

Optical Materials EXPRESS

has a proper structure length, its reflection dips and peaks will narrow down, improving the measurement accuracy. Its RI sensitivity in the low RI range of 1.332 ~1.387, which is more significant in chemical and biomedical sensing, reaches as high as 268.8 nm/RI unit (RIU), nine times higher than that of the fiber-taper-based Michelson interferometer RI sensor [19]. Moreover, the STFP is temperature-insensitive, making it a suitable candidate for temperature independent RI sensing.

2. Experimental methods

The schematic diagram of the STFP is shown in Fig. 1 (a). It consists of an S fiber taper and a silver mirror on the end facet. We first fabricated the SFT on a standard telecom single-mode fiber (SMF-28e, Corning, Inc.) by using a fusion splicer (Ericsson FSU-975). The detailed fabrication method was described in ref [22]. In our experiment, the discharge current, tapering time and axial offset of the fiber holders were set as 10 mA, 9 s and 150 μm, respectively. The obtained SFT was 725 μm in length and 62.5 μm in waist diameter. The axial offset is 100 μm [Fig. 1(b), inset]. Its transmission spectrum is shown in Fig. 2(a). The deepest attenuation peak is located at 1545 nm with an extinction ratio (attenuation difference of maximum and minimum value) of over 10 dB. Later, the SFT was cleaved and the silver mirror was fabricated on its end face. The fiber cleaving process was conducted under a microscope with a graduated scale on it in order to guarantee the flatness of the fiber end face and precisely control the length of the S-tapered fiber end-tip. The silver mirror was fabricated with chemical plating method. After cleaving, the cleaved fiber was dipped into the stannous chloride solution for several seconds to sensitize the surface of the fiber. Then the Tollens' reagent was prepared with a test tube and the temperature was set about 40 °C with water bath. In the end, the fiber was dipped in the test tube for 3 ~5 mins. In this way, a silver mirror with thickness of hundereds of nanometers was deposited on its end facet to form a fiber probe, as shown in the inset figure of Fig. 1(b). The opaque region on the fiber probe is silver coating. The silver mirror is used not only for enhancing the reflection (reflectivity R~80%) but also to protect the fiber end facet from contamination. The STFP was connected to a reflection-type optical path for RI sensing, as shown in Fig. 1(b). Light from a supercontinuum broadband light source (BBS) (Superk Compact, NKT Photonics, Inc.) propagates through a circulator and goes into the STFP. Then the reflected light passes through the circulator again and is collected by an optical spectrum analyzer (OSA) (Yokogawa AQ6370B) to monitor and record the reflection spectrum change.

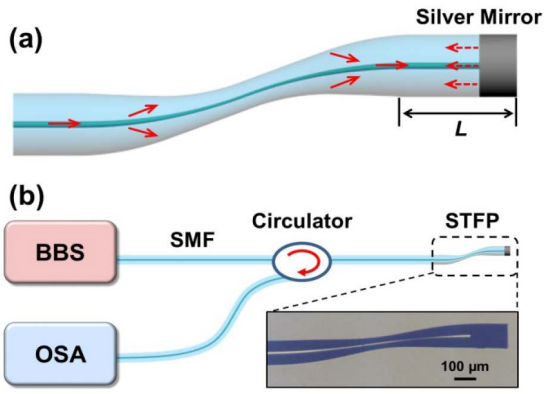

Fig. 1. (a) Schematic diagram of the STFP. (b) Experimental setup for RI sensing. Inset figure is the optical microscope image of the STFP.

Optical Materials EXPRESS

3. Results and discussions

3.1 Spectral characteristics and numerical simulation

The reflection spectrum of the STFP is dependent on the length of L from the end of SFT to silver mirror, as shown in Fig. 1(a). The obtained reflection spectra of the STFPs with different L of 10 mm, 375 μm, and 20 μm are plotted in Fig. 2(b)-(d), respectively. The number of attenuation peaks reduces with L decreasing. Actually, the light interference occurs twice in the STFP, which is similar but different with the double-pass in-line fiber taper MZI [20]. In the case of double-pass fiber taper MZI, the second interference derived from the reflected light just considers the core mode because the fiber pigtail is long enough to attenuate the cladding mode energy. However, in the STFP, the reflected cladding mode must be considered to participate in the second light interference, because the reflected cladding mode cannot be ignored due to the short length of L. So the whole interference process in the STFP is divided into two steps. Firstly, the input light propagates through the SFT and the first interference occurs, which can be simply described as the two-wave interference form

$$I_T = I_1 + I_2 + 2\sqrt{I_1 I_2}\cos(\Delta\Phi) \tag{1}$$

where I_1 and I_2 are the light intensities of the core mode and the cladding mode, and $\Delta\Phi$ is the phase difference between them. Here, $\Delta\Phi = 2\pi\Delta n_{eff} L_{eff}/\lambda$, where Δn_{eff} is the effective RI difference between the core and the cladding modes, L_{eff} is the effective length of the SFT interferometer, and λ is the input light wavelength.

In the next step, the second interference of the reflected light occurs in the SFT and the output light intensity is expressed as a three-wave interference form

$$I_R = I_1' + I_2' + I_{cl} + 2\sqrt{I_1' I_2'}\cos(\Delta\Phi_1) + 2\sqrt{I_1' I_{cl}}\cos(\Delta\Phi_2) + 2\sqrt{I_2' I_{cl}}\cos(\Delta\Phi_3) \tag{2}$$

where I_1' and I_2' are the light intensities of the core mode and the cladding mode in the SFT derived from the reflected core mode ($R \times I_T$), I_{cl} is the light intensity of the reflected cladding mode, $\Delta\Phi_1$, $\Delta\Phi_2$, and $\Delta\Phi_3$ are the phase differences between I_1', I_2' and I_{cl}, respectively. We believe that just one dominant cladding mode needs to be considered in the interference. Therefore, the light intensities of I_2' and I_{cl} correspond to the same high-order cladding mode. Except for the amplitude, the main difference between them is that they have the different phase. So the phase differences aforementioned can be expressed as $\Delta\Phi_1 = 2\pi\Delta n_{eff} L_{eff}/\lambda$, $\Delta\Phi_2 = 2\pi\Delta n_{eff}(L_{eff} + 2L)/\lambda$, $\Delta\Phi_3 = 0$, respectively. $\Delta\Phi_1$ has the same form as $\Delta\Phi$. For $\Delta\Phi_2$, the cavity length of the interferometer is $L_{eff} + 2L$, in which $2L$ represents the light passing through the L section twice due to the silver mirror reflection and L_{eff} represents the second interference in the SFT. Because the cladding modes of I_2' and I_{cl} have the same effective RI value, the effective RI difference between them is zero, resulting in $\Delta\Phi_3 = 0$. The transmission spectrum of the SFT and the reflection spectra of the STFPs with different L were simulated based on the above formulas. As shown in Figs. 3(a)-(d), the computed spectra are consistent with the experimental results [Figs. 2(a)-(d)].

Optical Materials EXPRESS

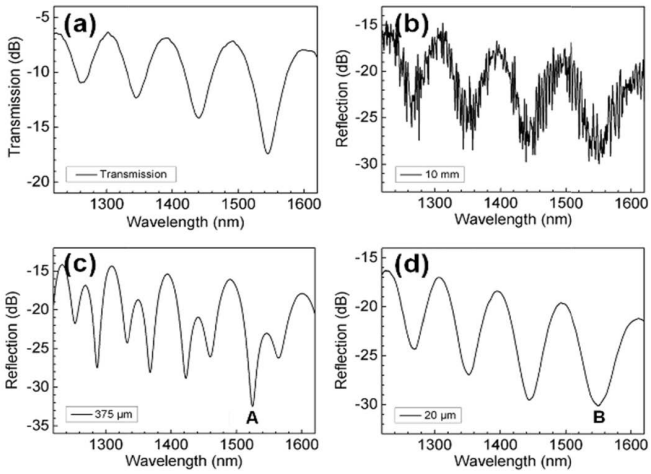

Fig. 2. (a) Transmission spectrum of the SFT. (b), (c), (d) Reflection spectra of the STFPs with L of 10 mm, 375 μm, and 20 μm, respectively.

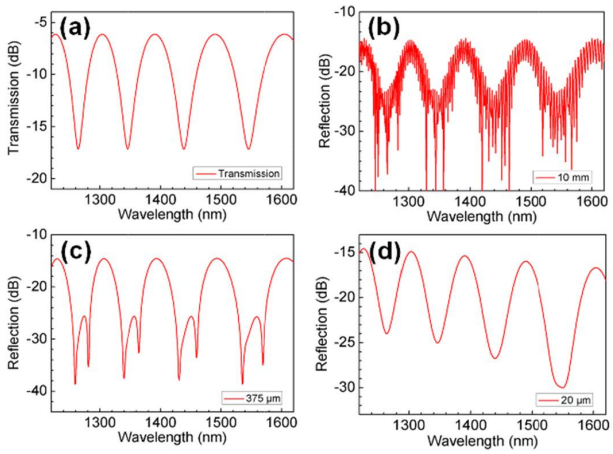

Fig. 3. (a) Computed transmission spectrum of the SFT. (b), (c), (d) Computed reflection spectra of the STFPs with L of 10 mm, 375 μm, 20 μm, respectively.

The reflection spectrum actually consists of a main and a secondary interferences. The main interference is dominantly controlled by the light intensities of I_1' and I_2', which are influenced by the geometrical parameters of the SFT and the silver mirror but are not affected by the length of L. The secondary interference is mainly influenced by the I_{cl} and L. In the case of Fig. 2(b), the periodicity of the main interference is defined by the phase difference $\Delta\Phi_1$. In addition, the relatively long L results in the dense resonance of the secondary interference. For Fig. 2(d), the L is so short that the phase difference of $\Delta\Phi_2$ is nearly the same as $\Delta\Phi_1$. So the secondary interference is negligible and the main periodicity of the interference is also determined by $\Delta\Phi_1$, making the reflection dip and peak wavelengths of Figs. 2(b) and (d) are about the same.

Optical Materials EXPRESS

When the length of L is shortening, the secondary interference peaks decrease and even disappear. So the relative short STFP has a simple reflection spectrum [Figs. 2(c) and (d)] and is good for sensor design. For Fig. 2(c), the narrow loss peaks used for sensing will enhance the measurement accuracy.

3.2 Sensing characteristics and discussions

The STFPs with *L* of 375 μm and 20 μm were chosen to test their RI responses at room temperature (20 °C). The STFPs were immersed in different concentrations of glycerin water solutions. The RI values of these solutions were calibrated by an Abbe refractometer at room temperature. We recorded the spectra change of attenuation peaks A and B [Figs. 2(c) and (d)] with different surrounding RI (SRI). The RI sensing results are shown in Fig. 4. Reflection spectra of the STFPs have a redshift with SRI increasing due to higher-order cladding mode, excited by the bending structure [21, 23], taking part in the light interference. Figures 4(b) and (d) show the wavelengths of peaks A and B change with SRI, respectively. The RI sensitivities in different RI ranges were also obtained. For peak A, in the RI ranges of 1.3320 ~1.4010, 1.4010 ~1.4146, and 1.4146 ~1.4216, the corresponding RI sensitivities are 158.7 nm/RIU, 323.5 nm/RIU, and 814.3 nm/RIU, respectively. The linearity is 0.993 through the linear fitting to the low RI range of 1.3320 ~1.4010. Its highest RI sensitivity is 1882.4 nm/RIU when the SRI changes between 1.4216 and1.4284. For peak B, in the RI range of 1.3320 ~1.3870, the RI sensitivity is 268.8 nm/RIU, which is 9 times higher than that of the reflective fiber-taper-based Michelson interferometer sensor [19], and the fitting linearity is 0.982. The other sensitivities are 562.1 nm/RIU, 908 nm/RIU, and 1760.3 nm/RIU in the RI ranges of 1.3870 ~1.4010, 1.4010 ~1.4216, and 1.4216 ~1.4284, respectively. The RI sensitivity augments with RI is owing to the cladding mode field expanding more energy to the environment with RI increasing, resulting in more sensitive response to SRI. Moreover, in order to improve the RI sensitivity of the sensor, we could minimize the waist diameter of the fiber to increase the evanescent field.

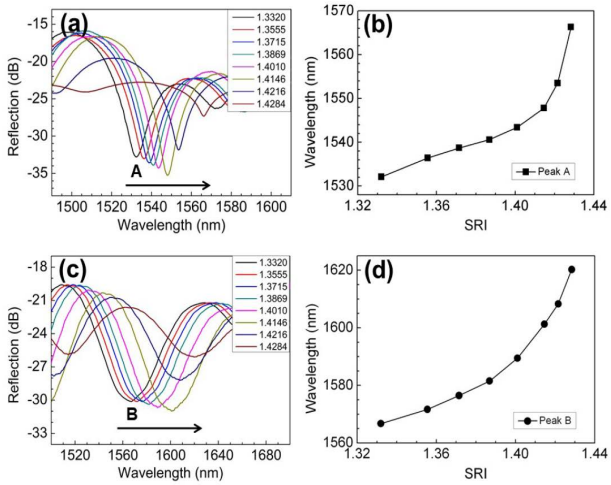

Fig. 4. (a) Reflection spectrum of the loss peak A changes with different SRI. (b) Relationship between the wavelength of peak A and SRI. (c) Reflection spectrum of the loss peak B changes with different SRI. (d) Relationship between the wavelength of peak B and SRI.

The thermal characteristic of the STFP is required and needs to be compensated in practical RI measurement, so we also investigated the temperature response of the STFP. The device was mounted on a hot plate, which was then heated up from room temperature to 100 °C in steps of 10 °C. The reflection spectrum of the STFP was nearly unchanged at different

Optical Materials EXPRESS

temperatures. The bottom wavelengths of loss peaks A and B just have random fluctuations with temperature, as shown in Fig. 5. Compared with the wavelength change with SRI, the temperature response of the STFP is negligible. This may be due to the combined effects of temperature induced RI change and thermal expansion induced axial strain variation in the SFT. The former drives the spectrum to move to longer wavelength but the latter pulls it back, making the two effects cancelled out. So the STFP is proper for the temperature independent RI sensing around room temperature.

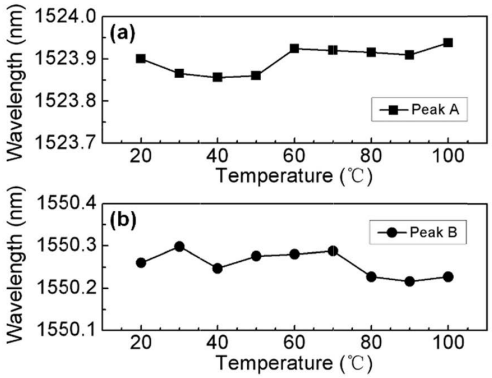

Fig. 5. (a), (b) Wavelengths of peak A and peak B change with temperature, respectively.

4. Conclusion

In conclusion, we have fabricated an S-tapered fiber probe for highly sensitive RI measurement. The STFP consists of an SFT and a silver mirror on the end facet. Its total length is about 1 mm, making it proper for sensing in narrow and small area. The reflection spectrum of the STFP has been discussed and simulated, and it is dependent on the total length of the structure. RI and temperature sensing experiments have been carried out. The results show that the STFP is temperature insensitive and has a RI sensitivity of 268.8 nm/RIU in the linear RI range of 1.3320 ~1.3870. This sensitive, low cost and simple structured RI sensor will find applications in chemical and biological sensing fields.

Funding

National Key Research and Development Program of China (No. 2017YFB1104300); National Natural Science Foundation of China (Nos. 61505206, 61590930, 91423102, 91323301, and 61435005); Science and Technology Development Project of Jilin Province (No. 20180201014GX).

Acknowledgment

C. Chen and R. Yang contributed equally to this work.